Arabian Journal of Chemistry (2023) 16, 104628

King Saud University

Arabian Journal of Chemistry

www.ksu.edu.sa
www.sciencedirect.com

ORIGINAL ARTICLE

Modeling and computational framework of radiative hybrid nanofluid configured by a stretching surface subject to entropy generation: Using Keller box scheme

Umar Farooq [a], Hassan Waqas [b], Musaad S. Aldhabani [c], Nahid Fatima [d], Abdullah Alhushaybari [e], Mohamed R. Ali [f,i,*], R. Sadat [g], Taseer Muhammad [h]

[a] Department of Mathematics, Government College University Faisalabad, 38000, Pakistan
[b] School of Energy and Power Engineering, Jiangsu University, Zhenjiang 212013, China
[c] Department of Mathematics, Faculty of Science, University of Tabuk, P.O.Box741, Tabuk 71491, Saudi Arabia
[d] Department of Mathematics and Sciences, Prince Sultan University, Riyadh 11586, Saudi Arabia
[e] Department of Mathematics, College of Science, Taif University, P.O. Box 11099, Taif 21944, Saudi Arabia
[f] Faculty of Engineering and Technology, Future University in Egypt, New Cairo 11835, Egypt
[g] Department of Mathematics, Faculty of Engineering, Zagazig University, Zagazig, Egypt
[h] Department of Mathematics, College of Sciences, King Khalid University, Abha 61413, Saudi Arabia
[i] Basic Engineering Science Department, Benha Faculty of Engineering, Benha University, Benha, Egypt

Received 11 November 2022; accepted 22 January 2023
Available online 27 January 2023

KEYWORDS

Hybrid nanofluid;
(Carbon nanotube;
Ferro);
Ethylene glycol base fluid;
Thermal radiation;
Entropy generation;
Mathematical physics;
Keller Box method;
MATLAB

Abstract This study examines the characteristics of the velocity, thermal field and entropy profiles for hybrid nanofluid flow passing through a starching sheet with thermal radiation. The carbon nanotube (SWCNT and MWCNT) are used as a nanoparticles with Cattaneo-Christov (C—C) heat flux. Ethylene glycol is utilized as a base fluid in this case. To achieve an improved solution, the fluid flow over the geometric properties is designed using highly non-linear PDEs, and the governing equations must be converted into dimensionless non-similar equation systems using the highly efficient well-known Keller-box scheme in computational software MATLAB. The practical feasibility of these solutions is determined by the range of the controlling parameters. The velocity distribution reduces as the magnetic parameter estimate increases, however, the temperature field and entropy production increase as the magnetic parameter fluctuation esclates. As the slip parameter is

* Corresponding author.
E-mail address: mohamed.reda@fue.edu.eg (M.R. Ali).

Peer review under responsibility of King Saud University.

Production and hosting by Elsevier

https://doi.org/10.1016/j.arabjc.2023.104628
1878-5352

increased, the velocity field diminish. The thermal field is enhanced for rising the radiation parameter, and the entropy profile is boosted for increasing Brinkman parameter values. The findings of this research might have a significant impact on industries where local cooling and heating via impingement jets are needed in electronic devices, heat sinks, drying technologies, and so on. To the best of the authors' knowledge, this is the first effort to employ a hybrid nanofluid to analyze entropy formation due to magnetohydrodynamics flow over a starching sheet.

Nomenclature

Symbols	Name with SI Unit		
(u, v)	Components of velocity $\left(ms^{-1}\right)$	(S)	Mass transfer parameter
(x, y)	Spatial coordinates(m)	(α_f)	Thermal diffusivity parameter
(k^*)	Mean absorption coefficient	(Gr)	Thermal radiation parameter
(t)	Time of hybrid nanofluid	(Ω)	Relaxation time parameter
(σ^*)	Stefan Boltzmann constant	(λ)	Velocity slip parameter
(T)	Temperature of surface (K)	(γ)	Biot number
(T_0)	Temperature of fluid (K)	$(SWCNT)$	Single-walled carbon nanotube
(W_1)	Velocity slip factor	(C_f)	Skin friction coefficient
(ρ_{hnf})	The density of hybrid nanofluid$\left(Kg/m^2\right)$	(Nu_x)	Local Nusselt number
(W_0)	Initial velocity parameter	$(\delta\&B)$	Column matrices
(V_w)	Porosity of sheet	(J)	Row matrices
(ρ)	Density$\left(Kgm^{-3}\right)$	(q_w)	Wall heat flux (K)
(k)	Thermal conductivity$\left(Wm^{-1}K^{-1}\right)$	(τ_w)	Shear stress tensor $\left(Nm^{-2}\right)$
(k_{hnf})	Thermal conductivity of hybrid nanofluid(W/mK)	(N_G)	Dimensionless entropy generation
(μ_{hnf})	The viscosity of hybrid nanofluid(Pa/s)	(ψ)	Stream function
(μ)	Dynamic viscosity$\left(Kgm^{-1}s^{-1}\right)$	(c)	Initial stretching rate
(ρC_p)	Heat capacitance $\left(Jm^{-3}K^{-1}\right)$	(Fe_3O_4)	Iron oxide (Ferro)
$(\rho C_p)_{hnf}$	Heat capacity of hybrid nanofluid(J/kgK)	$(i\&j)$	Component of deformation rate
$(\phi_1 = \phi_2)$	Nanoparticles volume fraction	$(MWCNT)$	Multi-walled carbon nanotube
$(\Pr)$	Prandtl number	$(\mu_{hnf}(B))$	Hybrid plastic dynamic viscosity
(A)	Unsteadiness parameter	(P_y)	Yield stress
(M)	Magnetic parameter	$\pi(= e_{ij}e_{ij})$	Product of deformation rate component
$()$	Temperature gradient	(π_c)	Critical value

1. Introduction

Nanoliquid is extremely crucial to researchers because of its increased heat transfer rates, which have substantial technological and manufacturing applications. Hybrid nanofluids are a form of fluid in which two or more metal particles are distributed in the base fluid. When contrasted to typical single-suspended fluids, this novel kind of nanofluid has exhibited intriguing advances in heat-transmitting qualities, in addition to thermo-physical and hydrodynamic properties. Hybrid nanofluids have a wide variety of implimentations in heat transmission, including transport, engineering, and biomedical science. The deferment of multiple nanomaterials in a base fluid mixture can be exploited to generate a hybrid nanofluid. Most natural activities are inextricably linked to nonlinearity, which is exceedingly difficult to resolve. It frequently requires irregular answers utilizing diverse strategies including numerical, approximation, or systematic ways to present an appropriate solution to the problem. Choi (Choi and Eastman, 1995) developed the theory of nanofluid. Kang et al. (Kang et al., 2006) introduced the new area of heat transfer and thermal conductivity is larger than that of single nanomaterials. The effects of a nanofluid along a curved channel containing nanoparticles and compliant walls were examined by Nadeem and Maraj (Nadeem and Maraj, 2014). Shaiq and Maraj (Shaiq and Maraj, 2019) scrutinized the significance of a magnetic field on a curved surface using a carbon nanotube. Maraj et al. (Maraj et al., 2018) studied the outcomes of nanoparticles with nanofluid and viscosity of nanoparticles. Maraj and Nadeem (Maraj and Nadeem, 2016) investigated the theoretical study of nanofluids in the occurence of heat radiation and nanoparticles in a channel. Maraj et al. (Maraj et al., 2022) introduced the MHD flow of a hybrid nanofluid including heat radiation and nanoparticles through a porous media. Li et al. (Li et al., 2020) developed the simulation of nanofluids containing motile microorganisms with bioconvection. Farooq et al. (Farooq et al., 2021) studied the stagnation point of nanoliquid in a rotating cylinder with an electromagnetic field. The free convectional flowing of hybrid Maxwell-based nanofluid via a channel generated by dual vertical plates has been recognized by Ahmad et al. (Ahmad et al., 2020). Hussanan et al. (Hussanan et al., 2020) estimated the enhancement of thermal transmission in non-Newtonian viscous plastics dependent flow across a sheet. Ghalambaz et al. (Ghalambaz et al., 2019) disclosed the movement and thermal transport of hybrid nanofluid in a compound shaped covered through a permeable Chanel. Thermal radiation has also performed a major role in the regulation of the thermal transfer process in the polymer industry. In a rotating phase, Chamkha et al. (Chamkha et al., 2019) witnessed the thermal transfer and the magneto-hydrodynamic motion of a hybrid nanofluid among two sheets. Waqas et al. (Waqas et al.,

2023) investigated the thermal transfer of the hybrid nanofluid through the numerical computational impact. Aziz et al. (Aziz et al., 2021) investigated Powell–Eyring water nanofluid, stream, convection thermal transfer, and volumetric entropy production. Zainal et al. (Zainal et al., 2020) investigate the flowing and thermal transmission kinds with a base of water nanofluid ($Al_2O_3 - Cu$) on a sheet. Rosca et al. (Roşca et al., 2020) provided the application of mathematical results for problems with the viscous kinematics flow of hybrid nanoparticles over a porous, non-linear, stretching sheet with a non-linear thermal radiation effect. The flow of a nanofluid in the occurence of nanoparticles and heat transfer was scrutinized by Muhammad et al. (Muhammad et al., 2021). Muhammad et al. (Muhammad et al., 2021) observed the numerical structure of a hybrid nanofluid consisting of nanoparticles and base fluid flowing past a curved sheet. Muhammad et al. (Muhammad et al., 2021) looked at the mixed convective flow of a hybrid nanofluid that included heat radiation and a carbon nanotube. Muhammad et al. (Muhammad et al., 2021) investigated the heat transfer of nanofluids and hybrid nanofluids across porous media. Hayat et al. (Hayat et al., 2021) explored hybrid nanofluids formed by combining convective and entropy production over a sheet. MHD focuses on the magnetic properties of electrical current fluids, like salt water, fluid metals, plasmas, and electrolytes. Magnetic fields can generate the force of Lorentz in a spinning fluid. It reduces the mobility of liquids and increases the concentration and temperature of nonmaterial. The role of the electromagnetic field is also important in the delayed separation of boundary layers MHD is also important in fields such as drug storing, manufacturing, mechanics, chemistry, and iron and steel, where it is used to treat cancer, asthma, cardiovascular, gastric drugs, electrodynamics cell division, optical transposable elements, magnetic properties resonance, copper wire stiffening, and optical devices. Nasir et al. (Nasir et al., 2020) compared the importance of heat transfer and thermal production/absorption of a stable MHD stagnation point water-base dater-based nanofluid over the cylinder. Tian et al. (Tian et al., 2021) identified the mixed convective thermal transmission as a combination of forced and natural convection. Biswas et al. (Biswas et al., 2021) illustrated an approach to improve thermal transport via porous materials subjected to thermal radiation during the MHD flow of the ($Al_2O_3 - Cu$) nanofluid. Daniel et al. (Daniel et al., 2019) studied the importance of MHD flow with convective properties of nanofluid. Daniel et al. (Daniel et al., 2017) introduced the thermal radiation influence of MHD and hybrid nanofluids. Daniel and Daniel (Daniel and Daniel, 2015) scrutinized the significance of heat radiation on a sheet-based MHD flow nanofluid. Daniel et al. (Daniel et al., 2017) analyzed the significance of entropy framework of nanofluid flow with heat radiation. Daniel et al. (Daniel et al., 2018) studied the upshot of MHD on hybrid nanofluid flow past through a variable thickness sheet. Daniel et al. (Daniel et al., 2017) introduced the nanofluid framework using MHD flow and stretch geometry heat transfer calculations. Using a chemical reaction sheet, Daniel et al. (Daniel et al., 2019) observed the effect of MHD with heat transfer in nanofluid.

The current research's main goal is to assess the relevance of a Ferro-based hybrid nanofluid including nanoparticles such as (*SWCNT, MWCNT,* and Fe_3O_4) and the base fluid ethylene glycol across a stretched sheet. The thermal radiation and Cattaneo-Christov (C—C) heat are applied to the current flow problem. To obtain the numerical and graphical results of the current investigation we use Bvp4c solver with the Keller box approach in the computational tool MATLAB. The different graphical outcomes are generated to deliberate the physical trend of prominent physical flow parameters via momentum profile, thermal profile, and entropy generation profile. The velocity field diminshies with rising magnetic parameter estimations, but the thermal field escalates with growing magnetic parameter values. The increasing variations of the velocity slip parameter declined the velocity profile and increased the thermal distribution profile. The current investigation can be expanded in the future to incorporate thermal radiation, entropy production, thermal conductivity, Cattaneo-Christov heat flow theory, and chemical processes. Moreover, the characteristics mentioned above might be added to other non-Newtonian models to examine their influence. There is always the possibility of carrying out practical examinations of such theoretical research. Furthermore, as a recommendation for future research in these domains, physical characteristics like density, viscosity, thermal conductivity, and so on are temperature dependent, which occurs when there is a considerable temperature differential inside the fluid.

2. Mathematical description

The flow of a two-dimensional hybrid nanofluid with thermal radiation and Cattaneo-Christov heat flux across a starching sheet was assumed in the current investigation. We also covered the consequences of entropy creation and slip effects in this section. Here we use the Ethylene Glycol (EG) base fluid ($SWCNT, MWCNT, Fe_3O_4$) as nanoparticles. Hybrid nanofluid flow is developed by stretching a sheet with $\left(B(t)\left(=\frac{B_0}{\sqrt{1-\varpi 1}}\right)\right)$ magnetic field strength embedded. The magnetic field is applied in the transverse direction of the surface. The velocity of the fluid is low due to the occurence of a magnetic field, hence the Ohmic dissipation and joule heating impacts are ignored. Here $\left(\left(\frac{1}{1-\varpi t}\right)\varpi t < 1\right)$ is effective stretching rate and (c) indicates the initial stretching rate. Fig. 1a depicts the geometry of flow model.

The hybrid plastic dynamic viscosity is symbolized by$\left(\mu_{hnf}(B)\right)$, the yield stress denoted by$\left(P_y\right)$,$(i\&j)$ are component of deformation rate, $\pi\left(= e_{ij}e_{ij}\right)$ which is a product of the deformation rate component and critical value(π_c).

The key assumptions of the current flow model are listed here:

- The problem of the two-dimensional hybrid nanofluid flow with thermal radiation is studied.
- The ($SWCNT - Fe_3O_4, MWCNT - Fe_3O_4$) nanoparticles and Ethylene Glycol base fluid are used here.
- The Cattaneo-Christov heat flux theory is highlighted.
- The entropy generation effect is also investigated here.
- The stretching surface shape geometry is analyzed.
- Here we use the Keller box method to obtain numerical and graphical outcomes of prominent parameters

The non-uniform velocity with the surface creates a flow (Jamshed and Aziz, 2018):

$$\left(U_w(x,t)\left(=\frac{cx}{1-\varpi t}\right)\right), \tag{1}$$

As the incompressible Casson nanofluid equation is (Oyelakin et al., 2016; Mukhopadhyay et al., 2013):

$$\left(\tau_{ij} = \begin{cases} 2\left(\mu_{hnf}(B) + \frac{p_y}{\sqrt{2\pi}}\right)e_{ij}, & \pi > \pi_c \\ 2\left(\mu_{hnf}(B) + \frac{p_y}{\sqrt{2\pi_c}}\right)e_{ij}, & \pi < \pi_c \end{cases}\right), \tag{2}$$

The vector forms of the governing equations are addressed as:

$$\rho_{hnf}\left(\frac{\partial q}{\partial t} + (q.\nabla)q\right) = -\nabla p + \mu_{hnf}\left(1 + \frac{1}{\beta}\right)\nabla^2 q + (J \times B)\Bigg\}, \tag{3}$$

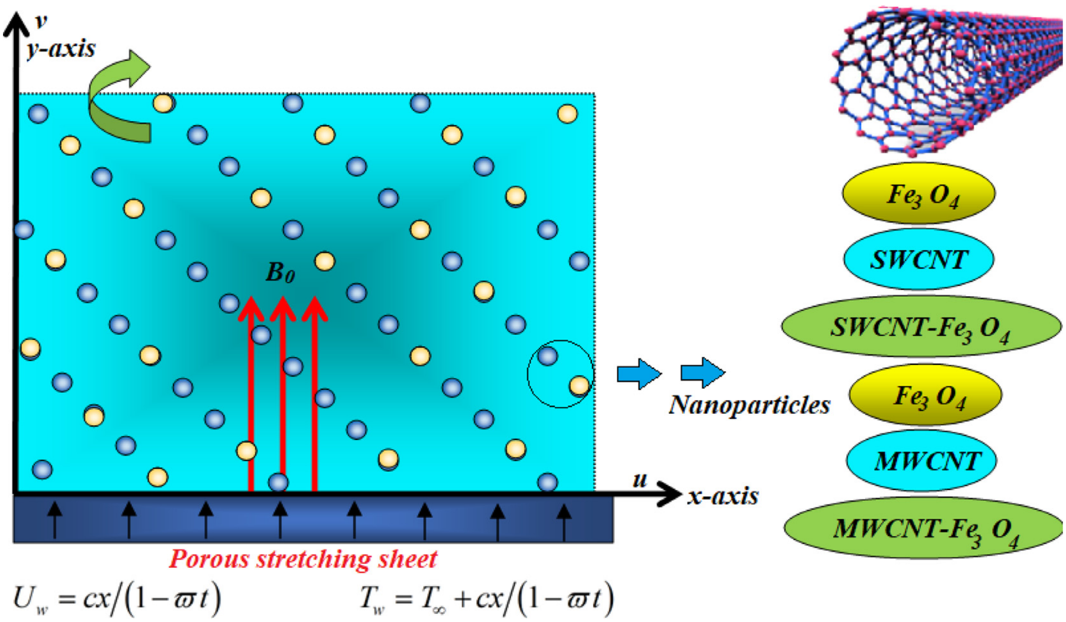

Fig. 1a Flow description of the problem.

$$(\rho c_p)_{hnf}\left(\frac{\partial T}{\partial t}+V.\nabla T\right)+\Gamma\left(\frac{\partial T}{\partial t}+v.\nabla q-q.\nabla v\right) \\ =\alpha_m\nabla^2 T-1/(\rho c)_f D_z q_r\Big\}, \tag{4}$$

The major equations are (Mustafa and Khan, 2015):

$$u_x+v_y=0\big\}, \tag{5}$$

$$u_t+uu_x+vu_y=\frac{\mu_{hnf}(B)}{\rho_{hnf}}u_{yy}-\frac{\sigma_{hnf}B^2(t)}{\rho_{hnf}}u\Big\}, \tag{6}$$

$$\left.\begin{array}{l} T_t+uT_x+vT_y+\Gamma\left[uu_xT_y+vv_yT_x+uv_xT_y+vu_yT_x\right. \\ \left.+u^2T_{xx}+v^2T_{yy}+2uvT_{xy}\right] \\ =\frac{k_{hnf}}{(\rho C_p)_{hnf}}\left[T_{yy}\right]-\frac{1}{(\rho C_p)_{hnf}}\left[q_{r_y}\right] \end{array}\right\}, \tag{7}$$

Here (λ_0) is constant in thermal relaxation factor is$\Gamma(=\lambda_0(1-\varpi t))$, (u,v) are velocities components in *x-axis* and *y-axis* direction. Here (t) is the time of the hybrid nanofluid; the velocity slip factor $W_1\left(=W_0\sqrt{1-\varpi t}\right)$ here (W_0) is the initial velocity parameter and V_w the porosity of the sheet.

These are the boundary conditions:

$$\left.\begin{array}{llll} u(x,0)=U_w+W_1\mu_{hnf}(B)(u_y), & & v(x,0)=V_w, & \\ & -k_f(T_y)=h(T_w-T), & & \\ u\to 0, & T\to T_\infty & as & y\to\infty \end{array}\right\}, \tag{8}$$

The following formula is used to determine the radiative heat flow (Brewster, 1992):

$$q_r=-\frac{4\sigma^*}{3k^*}T_y^*\Big\}, \tag{9}$$

In equation (9) the Stefan Boltzmann constant (σ^*) and the mean absorption coefficient are(k^*). The thermal difference inside the flow is assumed that (T^4) may be extended as a Taylor series around(T_∞). Here we use only linear terms.

$$T^4\cong 4T_\infty^3T-3T_\infty^4\big\}, \tag{10}$$

From equations (9) and (10):

$$q_{ry}=-\frac{16T_\infty^3\sigma^*}{3k^*}T_{yy}\Big\}, \tag{11}$$

Solving the main PDEs (05–08), here in analyze stream function as:

$$\left.\begin{array}{lll} u=\psi_y, & v=-\psi_x, & \zeta(x,y)=\sqrt{\frac{c}{v_f(1-\varpi t)}}y, \\ \psi(x,y)=\sqrt{\frac{v_fc}{(1-\varpi t)}}xf(\zeta), & & \theta(\zeta)=\frac{T-T_\infty}{T_w-T_\infty} \end{array}\right\}, \tag{12}$$

Using Eq. (12) and creating Table 1, the main PDEs converted into ODEs:

$$\left.\begin{array}{l} \frac{(1-\phi_1)^{-2.5}(1-\phi_2)^{-2.5}}{\left[(1-\phi_2)\left\{(1-\phi_1)+\phi_1\frac{\rho_{p1}}{\rho_f}\right\}\right]+\phi_2\frac{\rho_{p2}}{\rho_f}}f'''+ff''-f'^2-A\left(f'+\frac{\zeta}{2}f''\right)- \\ \frac{\left[1+\frac{3\left(\frac{\phi_1\sigma_{p1}+\phi_2\sigma_{p2}}{\sigma_f}-(\phi_1-\phi_2)\right)}{-\left(\frac{\phi_1\sigma_{p1}+\phi_2\sigma_{p2}}{\sigma_f}-(\phi_1+\phi_2)\right)+\left(\frac{\phi_1\sigma_{p1}+\phi_2\sigma_{p2}}{(\phi_1+\phi_2)\sigma_f}+2\right)}\right]}{\phi_2\frac{\rho_{p2}}{\rho_f}+\left[(1-\phi_2)\left\{(1-\phi_1)+\phi_1\frac{\rho_{p2}}{\rho_f}\right\}\right]}Mf'=0 \end{array}\right\}, \tag{13}$$

$$\left.\begin{array}{l} \theta''\left(1+\frac{k_f}{k_{hnf}}\mathrm{Pr}Gr\right)+\frac{k_f}{k_{hnf}}\mathrm{Pr}\left((1-\phi_2)\left\{\phi_1\frac{(\rho C_p)_{p1}}{(\rho C_p)_f}+(1-\phi_1)\right\}\right. \\ \left.+\frac{\phi_2(\rho C_p)_{p2}}{(\rho C_p)_f}\right) \\ \left[f\theta'-f'\theta-A\left(\theta+\frac{\zeta}{2}\theta'\right)-\Omega\left(f^2\theta''+ff'\theta'\right)\right]=0 \end{array}\right\}, \tag{14}$$

With

$$\left.\begin{array}{llll} f(0)=S, & f'(0)=1+\frac{\lambda}{(1-\phi_1)^{2.5}(1-\phi_1)^{2.5}}f''(0), & & \\ & \theta'(0)=-\gamma(1-\theta(0)), & & \\ f'(\zeta)\to 0, & \theta(\zeta)\to 0, & as & \zeta\to\infty \end{array}\right\}, \tag{15}$$

Table 1 Nanofluid and hybrid nanofluid physical characteristics (Shahzad et al., 2021; Ghadikolaei et al., 2017).

Properties	Nanofluid
Heat capacity	$\left((\rho c_p)_{nf}\left(\begin{matrix}=(\rho c_p)_f(1-\phi)\\+\phi(\rho c_p)_s\end{matrix}\right)\right)$
Thermal conductivity	$\left(\frac{k_{nf}}{k_f}\left(=\frac{k_s+k_f(m-1)-\phi(k_f-k_s)(m-1)}{k_s+(m-1)k_f+\phi(k_f-k_s)}\right)\right)$
Viscosity	$\left(\mu_{nf}(B)\left(=(1-\phi)^{2.5}\mu_f\right)\right)$
Density	$\left(\rho_{nf}\left(\begin{matrix}=\rho_f(1-\phi)\\+\phi\rho_s\end{matrix}\right)\right)$
Properties	**Hybrid nanofluid**
Heat capacity	$\left((\rho c_p)_{hnf}\left(\begin{matrix}=(1-\phi_2)\left[\begin{matrix}\phi_1(\rho c_p)_{p1}\\+(1-\phi_1)(\rho c_p)_f\end{matrix}\right]\\+\phi_2(\rho c_p)_{p2}\end{matrix}\right)\right)$
Thermal conductivity	$\left(\begin{matrix}\frac{k_{hnf}}{k_f}\left(=\frac{k_{s1}+(m-1)k_{hf}-(m-1)A_1(k_{hf}-k_{s1})}{k_{s1}+(m-1)k_{hf}+A_1(k_{hf}-k_{s1})}\right)\\\frac{k_{hnf}}{k_f}\left(=\frac{k_{s2}+(m-1)k_{hf}-(m-1)A_2(k_{hf}-k_{s2})}{k_{s2}+(m-1)k_{hf}+A_2(k_{hf}-k_{s2})}\right)\end{matrix}\right)$
Viscosity	$\left(\mu_{hnf}(B)\left(\begin{matrix}=\mu_f(1-A_1)^{2.5}\\(1-A_2)^{2.5}\end{matrix}\right)\right)$
Density	$\left(\rho_{hnf}\left(\begin{matrix}=(1-\phi_2)\left[\begin{matrix}(1-\phi_1)\rho_f\\+\phi_1\rho_{p1}\end{matrix}\right]\\+\phi_2\rho_{p2}\end{matrix}\right)\right)$

The prominent flow parameters are:

Parameter values	Parameter name	Notation
$A\left(=\frac{\varpi}{c}\right)$	Unsteadiness parameter	(A)
$M\left(=\frac{\sigma_f B_0^2}{c\rho_f}\right)$	Magnetic parameter	(M)
$\Omega(=c\Gamma)$	Relaxation time parameter	(Ω)
$\Pr\left(=\frac{v_f}{\alpha_f}\right)$	Prandtl number	$(\Pr)$
$\alpha_f\left(=\frac{K_f}{(\rho C_p)_f}\right)$	Thermal diffusivity parameter	(α_f)
$Gr\left(=\frac{16\sigma^* T_\infty^3}{3K^* v_f(\rho C_p)_f}\right)$	Thermal radiation parameter	(Gr)
$S\left(=-V_w\sqrt{\frac{1-\varpi t}{c v_f}}\right)$	Mass transfer parameter	(S)
$\lambda\left(=W_0\sqrt{\frac{c}{v_f}}\mu_f\right)$	Velocity slip parameter	(λ)
$\gamma\left(=\frac{h_f}{k_f}\sqrt{\frac{v_f(1-\varpi)t}{c}}\right)$	Biot number	(γ)
$Br\left(=\frac{\mu_f U_w^2}{k_f(T_w-T_\infty)}\right)$	Brinkman number	(Br)
$\left(=\frac{T_w-T_\infty}{T_\infty}\right)$	Temperature gradient	$()$
$Re\left(=\frac{U_w L^2}{v_f x}\right)$	Reynolds number	(Re)

3. Outcomes of the problem by Keller-box method

Because Eqs. (13)–(14) are non-linear, closed-form values are difficult to obtain. As a result, using the Keller-box technique, a finite-difference methodology, the equations with (15) are numerically resolved. Keller (Keller, 1971) devised the approach. This approach has been demonstrated to be very

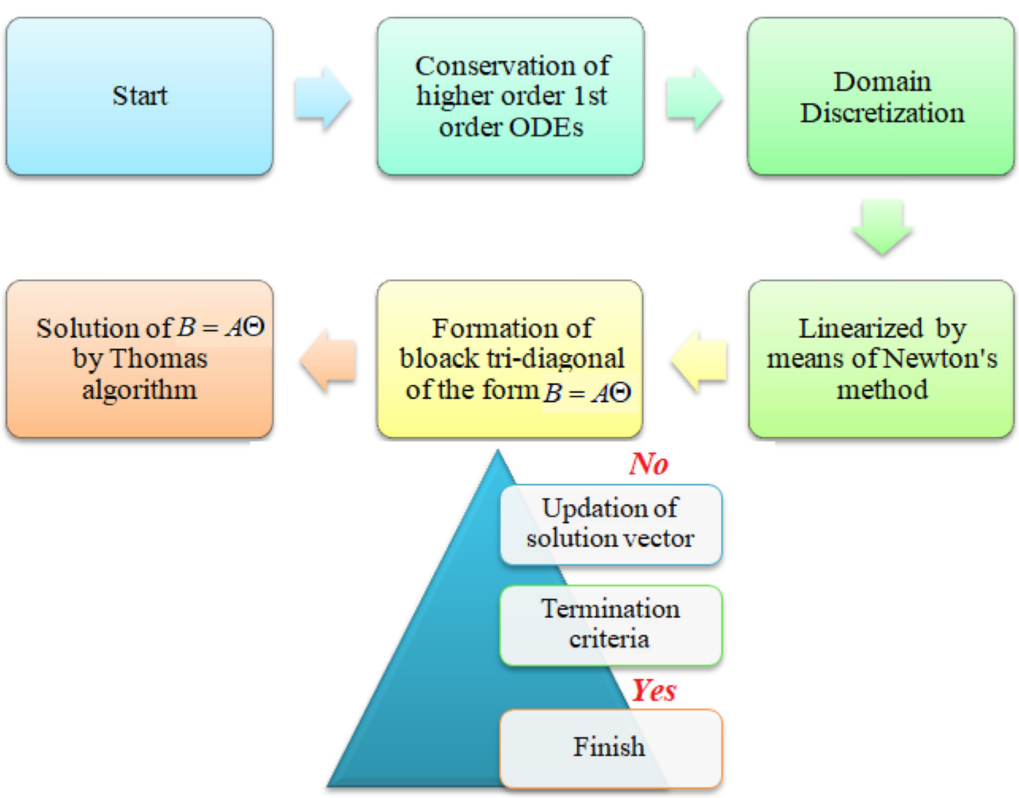

Fig. 1b KBM flow chart.

effective for parabolic issues. We employed the strategy provided by Cebeci and Pradshaw (Cebeci and Bradshaw, 2012), which has been proven to be particularly suited to dealing with non-linear situations and easily taken to numerically solve any kind of order. Fig. 1b shows the flow pattern of the given problem. The (KBM) Keller box method's main phases for obtaining approximate methods are as follows:

- Convert the provided first-order ordinary differential equations to a system.
- Simplified ODEs should be written in finite differences.
- Linearize the algebraic equations and express them in vector form employing Newton's approach.
- Use the block upper triangular elimination method to solve the linear system.

Here the 1st step of the method is to transfer ODEs (13)–(14) into 1st-order ODEs:

$$u=f', v=u', t=\theta'\}, \tag{16}$$

$$\left.\begin{array}{l}\frac{(1-\phi_1)^{-2.5}(1-\phi_2)^{-2.5}}{\left[(1-\phi_2)\left\{(1-\phi_1)+\phi_1\frac{\rho_{P1}}{\rho_f}\right\}\right]+\phi_2\frac{\rho_{P2}}{\rho_f}}v'-A\left(u+\frac{\zeta}{2}v\right)+fv-u^2\\ -\frac{\left[1+\frac{3\left(-(\phi_1-\phi_2)+\frac{\phi_1\sigma_{p1}+\phi_2\sigma_{p2}}{\sigma_f}\right)}{-\left(\frac{\phi_1\sigma_{p1}+\phi_2\sigma_{p2}}{\sigma_f}-(\phi_1+\phi_2)\right)+\left(\frac{\phi_1\sigma_{p1}+\phi_2\sigma_{p2}}{(\phi_1+\phi_2)\sigma_f}+2\right)}\right]}{\left[(1-\phi_2)\left\{(1-\phi_1)+\phi_1\frac{\rho_{p2}}{\rho_f}\right\}\right]+\phi_2\frac{\rho_{p2}}{\rho_f}}Mu=0\end{array}\right\}, \tag{17}$$

$$\left.\begin{array}{l}t'\left(1+\frac{k_f}{k_{hnf}}\mathrm{Pr}Gr\right)+\frac{k_f}{k_{hnf}}\mathrm{Pr}\left((1-\phi_2)\left\{(1-\phi_1)+\phi_1\frac{(\rho C_p)p_1}{(\rho C_p)_f}\right\}\right.\\ \left.+\frac{\phi_2(\rho C_p)p_2}{(\rho C_p)_f}\right)\\ \left[ft-u\theta-A\left(\theta+\frac{\zeta}{2}t\right)-\Omega\left(f^2t'+fut\right)\right]=0\end{array}\right\}, \tag{18}$$

With

$$\left.\begin{array}{lll}f=S, & u=1+\frac{\lambda}{(1-\phi_1)^{2.5}(1-\phi_1)^{2.5}}v, & \\ & t=-\gamma(1-\theta), & \\ u(\zeta)\to 0, & \theta(\zeta)\to 0, \quad as & \zeta\to\infty\end{array}\right\}, \tag{19}$$

As

$$\left.\begin{array}{ll}\zeta_0(=0), & \zeta_j(=\zeta_{j-1}+h),\\ & j(=1,2,3,\ldots)\\ j-1, & \zeta_j(=\zeta_\infty)\end{array}\right\},$$

The ODEs (16)–(18) are transferred into the non-linear algebraic form:

$$\left.\begin{array}{lll}\left(\frac{f_j-f_{j-1}}{h}\right) & = & \left(\frac{u_j+u_{j-1}}{2}\right),\\ \left(\frac{u_j-u_{j-1}}{h}\right) & = & \left(\frac{v_j+v_{j-1}}{2}\right),\\ \left(\frac{\theta_j-\theta_{j-1}}{h}\right) & = & \left(\frac{t_j+t_{j-1}}{2}\right)\end{array}\right\}, \tag{20}$$

$$\left.\begin{array}{l}\left(\frac{v_j+v_{j-1}}{h}\right)\frac{(1-\phi_1)^{-2.5}(1-\phi_2)^{-2.5}}{\left[(1-\phi_2)\left\{(1-\phi_1)+\phi_1\frac{\rho_{P1}}{\rho_f}\right\}\right]+\phi_2\frac{\rho_{P2}}{\rho_f}}-\left(\frac{u_j+u_{j-1}}{2}\right)^2-A\left\{\begin{array}{l}\left(\frac{u_j+u_{j-1}}{2}\right)+\\ \frac{\zeta}{2}\left(\frac{v_j+v_{j-1}}{2}\right)\end{array}\right\}\\ +\left(\begin{array}{c}\left(\frac{v_j+v_{j-1}}{2}\right)\\ \left(\frac{f_j+f_{j-1}}{2}\right)\end{array}\right)-\left(\begin{array}{c}\frac{\left[1+\frac{3\left(-(\phi_1-\phi_2)+\frac{\phi_1\sigma_{p1}+\phi_2\sigma_{p2}}{\sigma_f}\right)}{-\left(-(\phi_1+\phi_2)+\frac{\phi_1\sigma_{p1}+\phi_2\sigma_{p2}}{\sigma_f}\right)+\left(\frac{\phi_1\sigma_{p1}+\phi_2\sigma_{p2}}{(\phi_1+\phi_2)\sigma_f}+2\right)}\right]}{\left[(1-\phi_2)\left\{(1-\phi_1)+\phi_1\frac{\rho_{p2}}{\rho_f}\right\}\right]+\phi_2\frac{\rho_{p2}}{\rho_f}}\\ M\left(\frac{u_j+u_{j-1}}{2}\right)\end{array}\right)=0\end{array}\right\}, \tag{21}$$

$$\left.\begin{array}{l}\left(\frac{t_j+t_{j-1}}{h}\right)\left(1+\frac{k_f}{k_{hnf}}\mathrm{Pr}Gr\right)+\frac{k_f}{k_{hnf}}\mathrm{Pr}\left(\left(\frac{\phi_2(\rho C_p)p_2}{(\rho C_p)_f}\right)\right.\\ \left.\quad+(1-\phi_2)\left\{(1-\phi_1)+\phi_1\frac{(\rho C_p)p_1}{(\rho C_p)_f}\right\}\right)\\ \left[\begin{array}{c}-\left(\frac{\theta_j+\theta_{j-1}}{2}\right)\left(\frac{u_j+u_{j-1}}{2}\right)+\left(\frac{t_j+t_{j-1}}{2}\right)\frac{f_j+f_{j-1}}{2}-A\left\{\left(\frac{\theta_j+\theta_{j-1}}{2}\right)+\frac{\zeta}{2}\left(\frac{t_j+t_{j-1}}{2}\right)\right\}\\ -\Omega\left(\left(\frac{t_j-t_{j-1}}{h}\right)\left(\frac{f_j+f_{j-1}}{2}\right)^2+\left(\frac{f_j+f_{j-1}}{2}\right)\left(\frac{u_j+u_{j-1}}{2}\right)\left(\frac{t_j+t_{j-1}}{2}\right)\right)\end{array}\right]=0\end{array}\right\}, \tag{22}$$

In the above *(i + 1)* iteration, so

$$()_j^{(i+1)}=()_j^{(i)}+\Theta()_j^{(i)}\} \tag{23}$$

By sub Eqs. (20)–(22) we get

$$\left.\begin{array}{l}\left(\Theta f_j-\frac{1}{2}h\left(\Theta u_j+\Theta f_{j-1}\right)-\Theta f_{j-1}\right)=(R_1)_{j-\frac{1}{2}}\\ \left(\Theta u_j-\frac{1}{2}h\left(\Theta v_j+\Theta v_{j-1}\right)-\Theta u_{j-1}\right)=(R_2)_{j-\frac{1}{2}}\\ \left(\Theta\theta_j-\frac{1}{2}h\left(\Theta t_j+\Theta t_{j-1}\right)-\Theta\theta_{j-1}\right)=(R_3)_{j-\frac{1}{2}}\end{array}\right\} \tag{24}$$

$$\left.\begin{array}{l}\left(\begin{array}{c}\Theta f_j(a_1)_j+\Theta f_{j-1}(a_2)_j+\Theta u_j(a_3)_j+\Theta u_{j-1}(a_4)_j+\Theta u_{j-1}(a_4)_j\\ +\Theta v_j(a_5)_j\\ +\Theta v_{j-1}(a_6)_j+\Theta\theta_j(a_7)_j+\Theta\theta_j(a_8)_j+\Theta t_j(a_9)_j+\Theta t_{j-1}(a_{10})_j\end{array}\right)=(R_4)_{j-\frac{1}{2}}\\ \left(\begin{array}{c}\Theta f_j(b_1)_j+\Theta f_{j-1}(b_2)_j+\Theta u_j(b_3)_j+\Theta u_{j-1}(b_4)_j+\Theta u_{j-1}(b_4)_j\\ +\Theta v_j(b_5)_j\\ +\Theta v_{j-1}(b_6)_j+\Theta\theta_j(b_7)_j+\Theta\theta_j(b_8)_j+\Theta t_j(b_9)_j+\Theta t_{j-1}(b_{10})_j\end{array}\right)=(R_5)_{j-\frac{1}{2}}\end{array}\right\} \tag{25}$$

Here

$$\left(\left(-f_j+\frac{h}{2}(u_j+u_{j-1})+f_{j-1}\right)=(R_1)_{j-\frac{1}{2}}\right), \tag{26}$$

$$\left(\left(-u_j+\frac{h}{2}(v_j+v_{j-1})+u_{j-1}\right)=(R_2)_{j-\frac{1}{2}}\right), \tag{27}$$

$$\left(\left(-\theta_j+\frac{h}{2}(t_j+t_{j-1})+\theta_{j-1}\right)=(R_3)_{j-\frac{1}{2}}\right), \tag{28}$$

$$\left.\left(\begin{array}{l}\left[\left(\frac{(v_j+v_{j-1})(f_j+f_{j-1})}{4}\right)+\frac{(1-\phi_1)^{-2.5}(1-\phi_2)^{-2.5}}{\left[(1-\phi_2)\left\{(1-\phi_1)+\phi_1\frac{\rho_{P1}}{\rho_f}\right\}\right]+\phi_2\frac{\rho_{P2}}{\rho_f}}\left(\frac{v_j+v_{j-1}}{h}\right)\right]\\ -h\left(-M\frac{\phi_4}{\phi_2}\left(\frac{u_j+u_{j-1}}{2}\right)-A\left(\left(\frac{u_j+u_{j-1}}{2}\right)+\zeta\left(\frac{v_j+v_{j-1}}{4}\right)\right)-\left(\frac{u_j+u_{j-1}}{2}\right)^2\right)\end{array}\right)=(R_4)_{j-\frac{1}{2}}\right\}, \tag{29}$$

$$\left.\begin{pmatrix} -h\left[\left(\frac{t_j+t_{j-1}}{h}\right)\left(1+\frac{k_f}{k_{hnf}}\mathrm{Pr}Gr\right)\right] \\ -h\frac{k_f}{k_{hnf}}\mathrm{Pr}\left((1-\phi_2)\left\{(1-\phi_1)+\phi_1\frac{(\rho C_p)_{p1}}{(\rho C_p)_f}\right\}+\frac{\phi_2(\rho C_p)_{p2}}{(\rho C_p)_f}\right) \\ \left[\left(\frac{(t_j+t_{j-1})(f_j+f_{j-1})}{4}\right)\right]+h\frac{k_f}{k_{hnf}}\mathrm{Pr}\begin{pmatrix}\left\{(1-\phi_1)+\phi_1\frac{(\rho C_p)_{p1}}{(\rho C_p)_f}\right\}(1-\phi_2) \\ +\frac{\phi_2(\rho C_p)_{p2}}{(\rho C_p)_f}\end{pmatrix} \\ \left[\left(\frac{(u_j+u_{j-1})(t_j+t_{j-1})}{4}\right)\right]+Ah\frac{k_f}{k_{hnf}}\mathrm{Pr}\begin{pmatrix}\left\{(1-\phi_1)+\phi_1\frac{(\rho C_p)_{p1}}{(\rho C_p)_f}\right\}(1-\phi_2) \\ +\frac{\phi_2(\rho C_p)_{p2}}{(\rho C_p)_f}\end{pmatrix} \\ \left[\left(\frac{\theta_j+\theta_{j-1}}{2}\right)\right]+Ah\frac{k_f}{k_{hnf}}\mathrm{Pr}\left((1-\phi_2)\left\{(1-\phi_1)+\phi_1\frac{(\rho C_p)_{p1}}{(\rho C_p)_f}\right\}+\frac{\phi_2(\rho C_p)_{p2}}{(\rho C_p)_f}\right) \\ \left[\left(\frac{t_j+t_{j-1}}{2}\right)\right]+\Omega h\frac{k_f}{k_{hnf}}\mathrm{Pr}\left[\left(\frac{t_j+t_{j-1}}{h}\right)\left(\frac{f_j+f_{j-1}}{2}\right)^2\right] \\ \begin{pmatrix}(1-\phi_2)\left\{(1-\phi_1)+\phi_1\frac{(\rho C_p)_{p1}}{(\rho C_p)_f}\right\} \\ +\frac{\phi_2(\rho C_p)_{p2}}{(\rho C_p)_f}\end{pmatrix}+\Omega h\frac{k_f}{k_{hnf}}\mathrm{Pr}\begin{bmatrix}\left(\frac{u_j+u_{j-1}}{2}\right) \\ \left(\frac{f_j+f_{j-1}}{2}\right)\end{bmatrix}\left[\left(\frac{t_j+t_{j-1}}{2}\right)\right] \\ \left((1-\phi_2)\left\{(1-\phi_1)+\phi_1\frac{(\rho C_p)_{p1}}{(\rho C_p)_f}\right\}+\frac{\phi_2(\rho C_p)_{p2}}{(\rho C_p)_f}\right) \end{pmatrix}=(R_5)_{j-\frac{1}{2}}\right\}, \tag{30}$$

Finally, the boundaries are:

$$\left.\begin{matrix}\Theta f_0(=0), & & \Theta u_0(=0), \\ & \Theta t_0(=0), & \\ \Theta u_j(=0), & & \Theta\theta_j(=0)\end{matrix}\right\}, \tag{31}$$

The linear Eqs. (24)–(25) in matrix form:

$$B=A\Theta, \tag{32}$$

$$B=\begin{bmatrix}(R_1)_{j-\frac{1}{2}} \\ (R_2)_{j-\frac{1}{2}} \\ \vdots \\ (R_{J-1})_{j-\frac{1}{2}} \\ (R_J)_{j-\frac{1}{2}}\end{bmatrix}, A=\begin{bmatrix}a_1 & c_1 & & & \\ b_2 & a_2 & c_2 & & \\ & \ddots & \ddots & \ddots & \\ & & b_{j-1} & a_{J-1} & c_{J-1} \\ & & b_j & a_j & a\end{bmatrix},$$

$$\Theta=\begin{bmatrix}\Theta_1 \\ \Theta_2 \\ \vdots \\ \Theta_{J-1} \\ \Theta_J\end{bmatrix}, \tag{33}$$

Here, (A) is the block tri-diagonal matrix which is denoted by $(J\times J)$ the size of the block(5×5). The column matrices are symbolized by$(\Theta\&B)$. The row of matrices is denoted by(J). To explain the linear scheme (Θ) the LU factorization method can be used.

The physical quantities are:

$$\left.\begin{matrix}C_f\left(=\frac{\tau_w}{\rho_f U_w^2}\right), \\ Nu_x\left(=\frac{xq_w}{k_f(T_w-T_\infty)}\right)\end{matrix}\right\}, \tag{34}$$

Where

$$\left.\begin{matrix}\tau_w\left(=-\left(\mu_{hnf}(B)+\frac{p_y}{\sqrt{2\pi}}\right)(u_y)_{y=0}\right), \\ q_w\left(=-k_{nf}\left(1+\frac{16\sigma^* T_\infty^3}{3k^* k_f}\right)(T_y)_{y=0}\right)\end{matrix}\right\}, \tag{35}$$

The results of physical quantities:

$$\left.\begin{matrix}C_f Re_x^{\frac{1}{2}}\left(=-\frac{f''(0)}{(1-\phi_1)^{2.5}(1-\phi_2)^{2.5}}\right), \\ Nu_x Re_x^{-\frac{1}{2}}\left(=-\frac{k_{hnf}}{k_f}(1+Gr)\theta'(0)\right)\end{matrix}\right\}, \tag{36}$$

4. Entropy generation analysis

The mathematical model with entropy generation is written as (Keller, 1971):

$$uE_G=\frac{k_{hnf}}{T_\infty^2}\left\{(T_y)^2+\frac{16\sigma^* T_\infty^3}{3k^*}(T_y)^2\right\}+\frac{\mu_{hnf}(B)}{T_\infty}(u_y)^2+\frac{\sigma_{hnf}B^2(t)u^2}{T_\infty}\Bigg\}, \tag{37}$$

The dimensionless entropy generation is written as:

$$N_G\left(=\frac{T_\infty^2 c^2 E_G}{k_f(T_w-T_\infty)}\right), \tag{38}$$

The dimensionless form of entropy can be written by using Eq. (12).

$$NRe\left(\frac{k_{hnf}}{k_f}(1+Gr)\theta'^2\right)+\frac{1}{(1-\phi_1)^{2.5}(1-\phi_2)^{2.5}}\frac{B_r Re}{}\left(f''^2\right)$$
$$+\frac{B_r Re}{}\left(\left[1+\frac{\frac{3(\phi_1\sigma_{p1}+\phi_2\sigma_{p2})}{\sigma_f}-(\phi_1+\phi_2)}{\frac{(\phi_1\sigma_{p1}+\phi_2\sigma_{p2})}{(\phi_1+\phi_2)\sigma_f}-\frac{(\phi_1\sigma_{p1}+\phi_2\sigma_{p2})}{\sigma_f}-(\phi_1+\phi_2)}\right]Mf'^2\right), \tag{39}$$

Where

$$Re\left(=\frac{U_w L^2}{v_f x}\right),\ Br\left(=\frac{\mu_f U_w^2}{k_f(T_w-T_\infty)}\right),\left(=\frac{T_w-T_\infty}{T_\infty}\right)\Bigg\}, \tag{40}$$

5. Results and discussion

In this section, we investigated the graphical and numerical findings of prominent flow parameter via momentum profile, thermal profile, and entropy profile via a well-known numerical approach (KBM) Keller box method in the well Known software computational MATLAB. The significance of the magnetic parameter (M) via the velocity distribution $f'(\zeta)$ is seen in Fig. 2**.** The dimensionless velocity profile $f'(\zeta)$ decreased with the (M) increases. According to the Lorentz force, the magnetic field introduces a retarding body force that controverts the direction of the external magnetic field. When the magnetic parameter amount is higher, the retarding body is continuously on the rise, and the dimensionless velocity drops. Furthermore, when the magnetic field rises, the extent of the boundary layer declines. Fig. 3 examines the characteristics of (λ) The velocity field $f'(\zeta)$ the velocity field f' is decreased for the increasing value of the velocity slip parameter (λ) for various shape factors of nanoparticles$(SWCNT - Fe_3O_4, MWCNT - Fe_3O_4)$. Fig. 4 reveals the characteristics of the volumetric fraction of nanoparticles $(\phi_1 = \phi_2)$ via velocity profile$f'(\zeta)$. The velocity field $f'(\zeta)$ declined for the increasing magnitude of $(\phi_1 = \phi_2)$ for various shape factors of nanoparticles with $(SWCNT - Fe_3O_4, MWCNT - Fe_3O_4)$ and base fluid is (EG) ethylene glycol. Fig. 5 shows the impact of the temperature profile $\theta(\zeta)$ on the magnetic parameter(M). We analyze that the $\theta(\zeta)$ is enhanced for the booming variations of the(M). Fig. 6 characterizes the consequence of slip parameter (λ) against the temperature filed$\theta(\zeta)$. This diagram shows how raising the (λ) improves temperature filed$\theta(\zeta)$. Fig. 7 deliberates the features of radiation parameter (Gr) on the thermal filed$\theta(\zeta)$. It is observed that the $\theta(\zeta)$ rises with an improvement in (Gr) various shape factors of nanoparticles with hybrid particles and the base fluid is (EG) ethylene glycol. Fig. 8 includes temperature distribution filed $\theta(\zeta)$ against (γ) when the curvature parameter is used for various form variables of nanoparticles in both instances with $(SWCNT - Fe_3O_4, MWCNT - Fe_3O_4)$ and base fluid is ethylene glycol. It is found that temperature distribution filed $\theta(\zeta)$ a curve goes up with enhances in the magnitude of(γ). Fig. 9 illustrates the impact of $(\phi_1 = \phi_2)$ various shape factors of

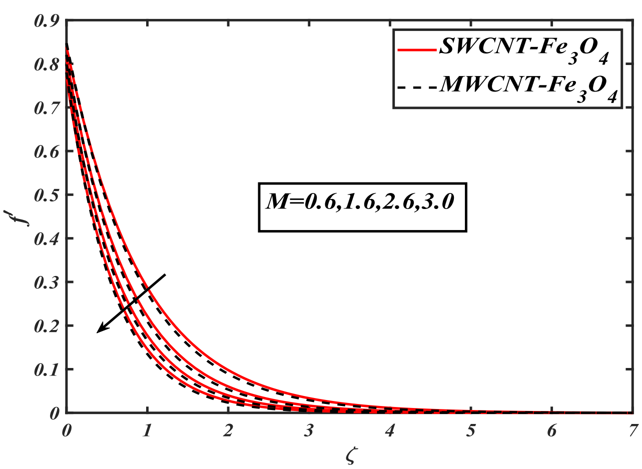

Fig. 2 Findings of (M) on velocity field for$(SWCNT - Fe_3O_4, MWCNT - Fe_3O_4)$.

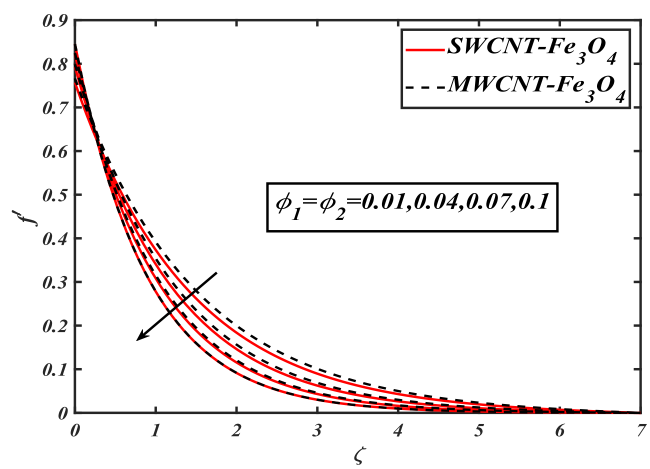

Fig. 4 Findings of $(\phi_1 = \phi_2)$ on velocity field for$(SWCNT - Fe_3O_4, MWCNT - Fe_3O_4)$.

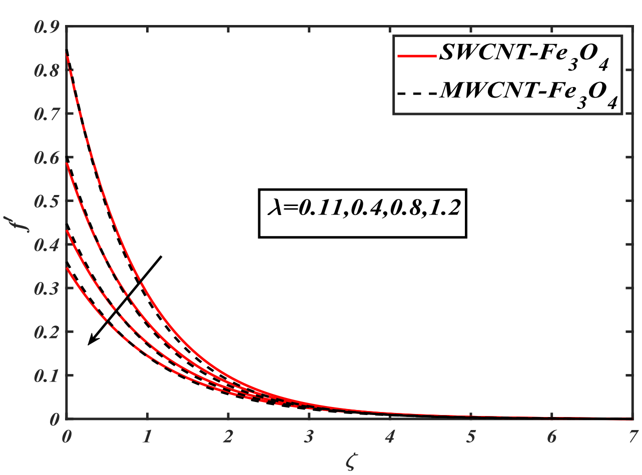

Fig. 3 Findings of (λ) on velocity field for$(SWCNT - Fe_3O_4, MWCNT - Fe_3O_4)$.

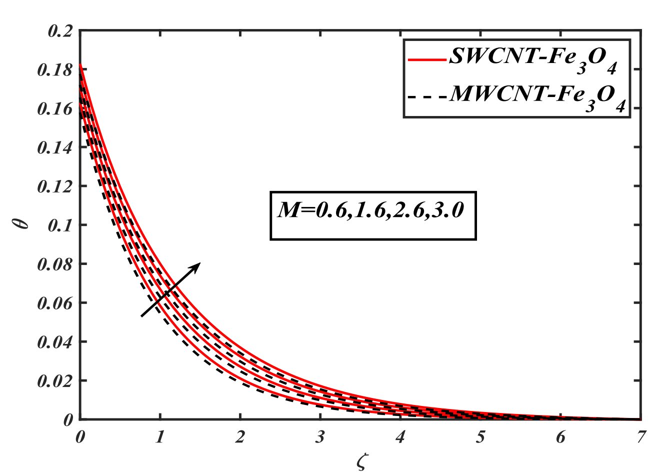

Fig. 5 Findings of (M) on heat field for$(SWCNT - Fe_3O_4, MWCNT - Fe_3O_4)$.

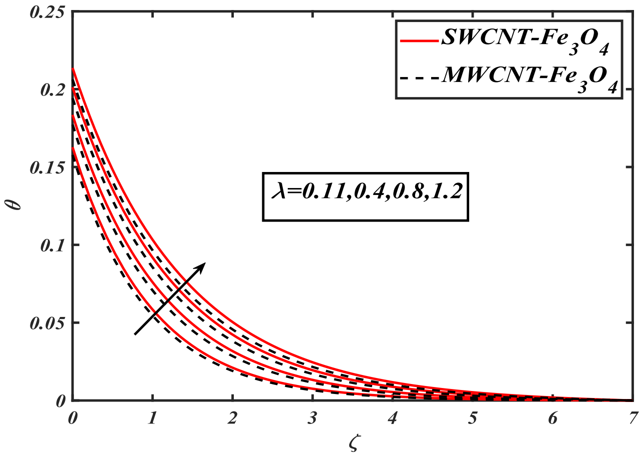

Fig. 6 Findings of (λ) on heat field for$(SWCNT - Fe_3O_4, MWCNT - Fe_3O_4)$.

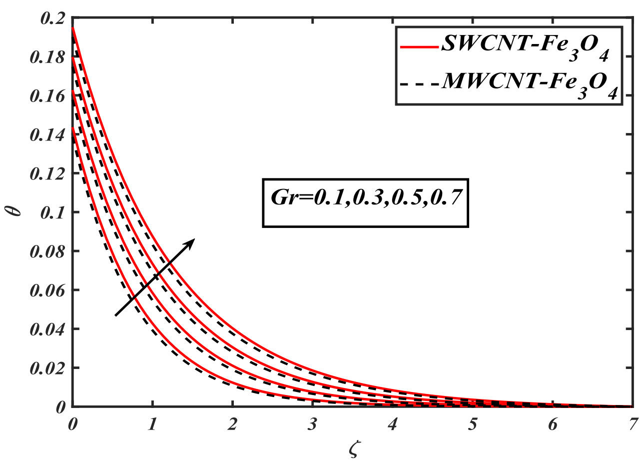

Fig. 7 Findings of (Gr) on heat field for$(SWCNT - Fe_3O_4, MWCNT - Fe_3O_4)$.

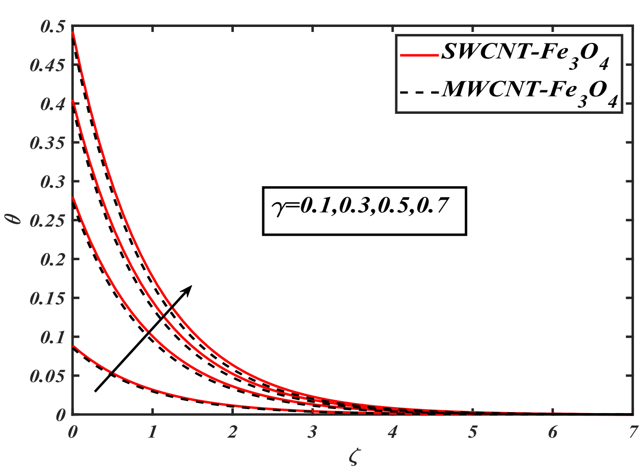

Fig. 8 Findings of (γ) on heat field for$(SWCNT - Fe_3O_4, MWCNT - Fe_3O_4)$.

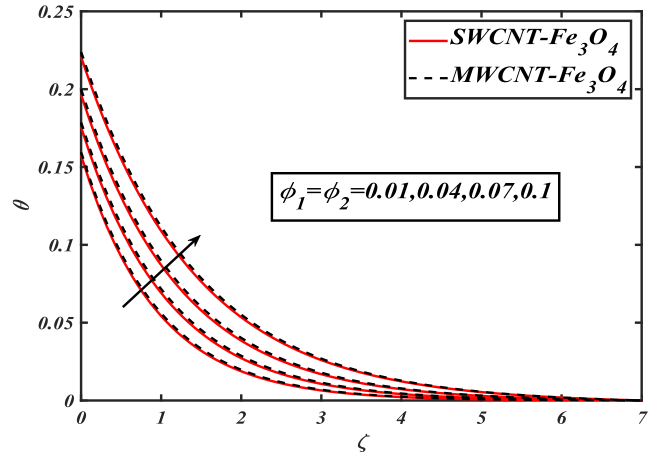

Fig. 9 Findings of $(\phi_1 = \phi_2)$ on heat field for$(SWCNT - Fe_3O_4, MWCNT - Fe_3O_4)$.

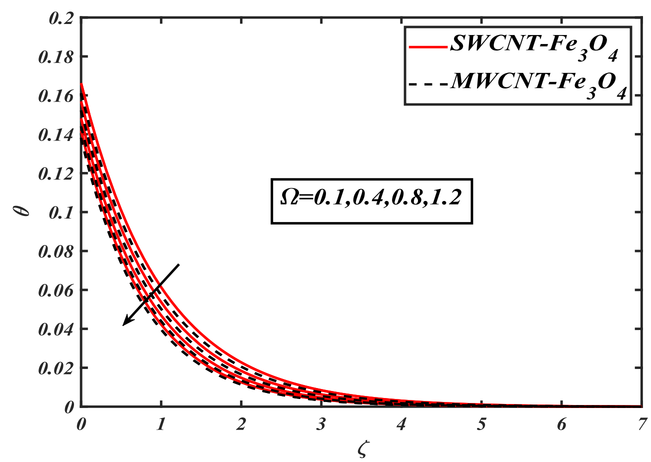

Fig. 10 Findings of (Ω) on heat field for$(SWCNT - Fe_3O_4, MWCNT - Fe_3O_4)$.

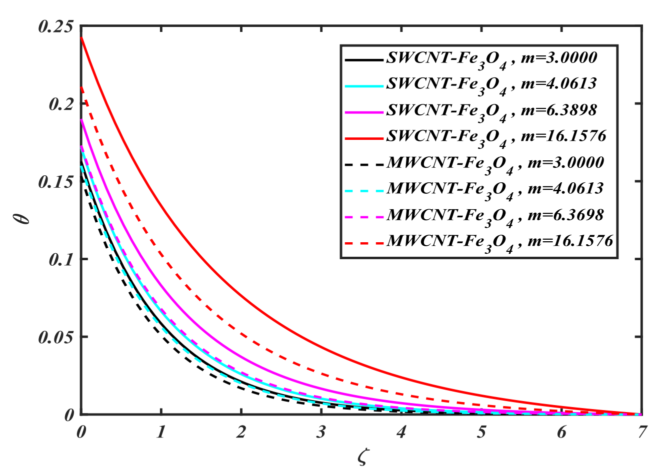

Fig. 11 Findings of (m) on heat field for$(SWCNT - Fe_3O_4, MWCNT - Fe_3O_4)$.

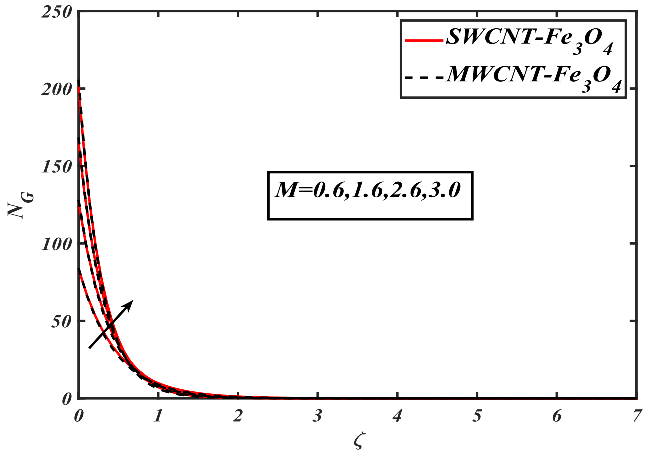

Fig. 12 Findings of (M) on entropy field for$(SWCNT-Fe_3O_4, MWCNT-Fe_3O_4)$.

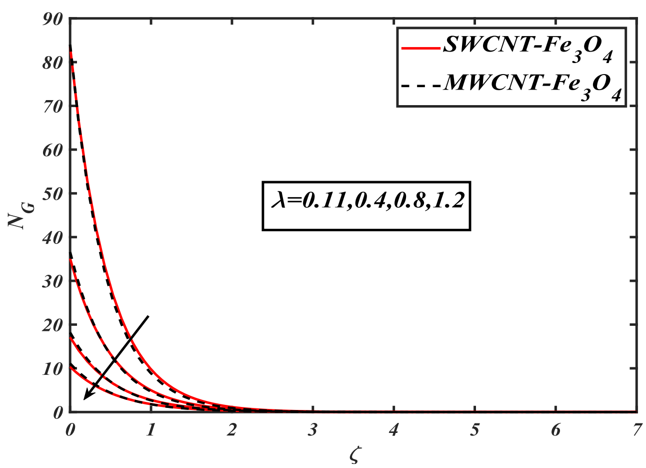

Fig. 13 Findings of (λ) on entropy field for$(SWCNT-Fe_3O_4, MWCNT-Fe_3O_4)$.

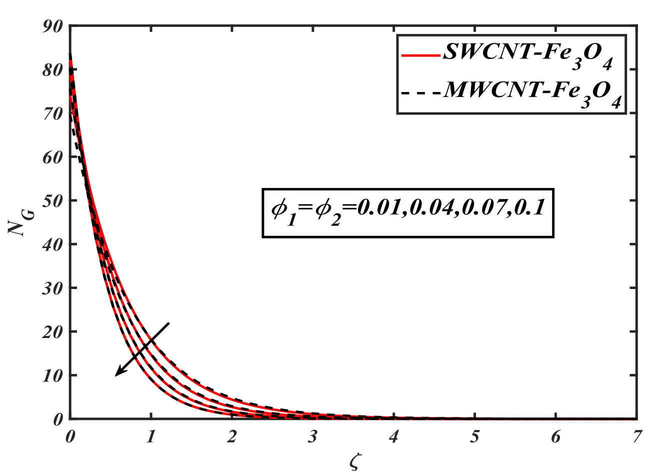

Fig. 14 Findings of $(\phi_1 = \phi_2)$ on entropy field for$(SWCNT-Fe_3O_4, MWCNT-Fe_3O_4)$.

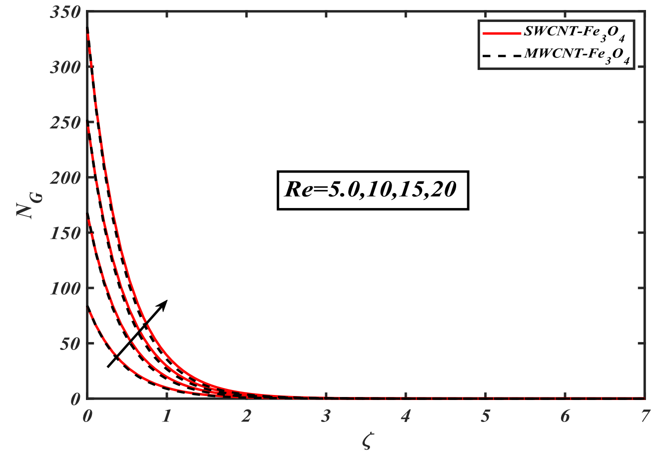

Fig. 15 Findings of (Re) on entropy field for$(SWCNT-Fe_3O_4, MWCNT-Fe_3O_4)$.

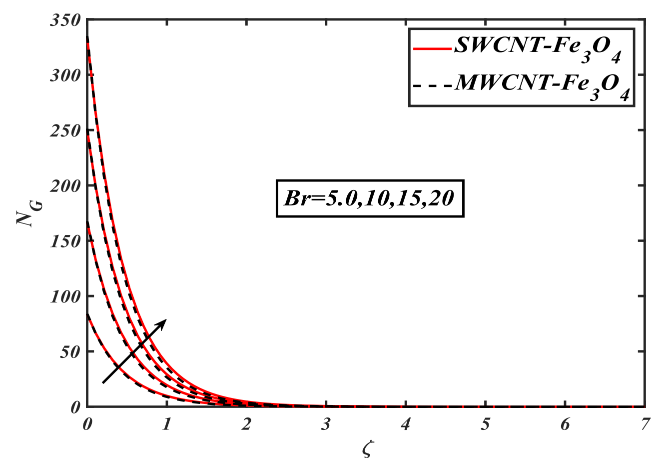

Fig. 16 Findings of (Br) on entropy field for$(SWCNT-Fe_3O_4, MWCNT-Fe_3O_4)$.

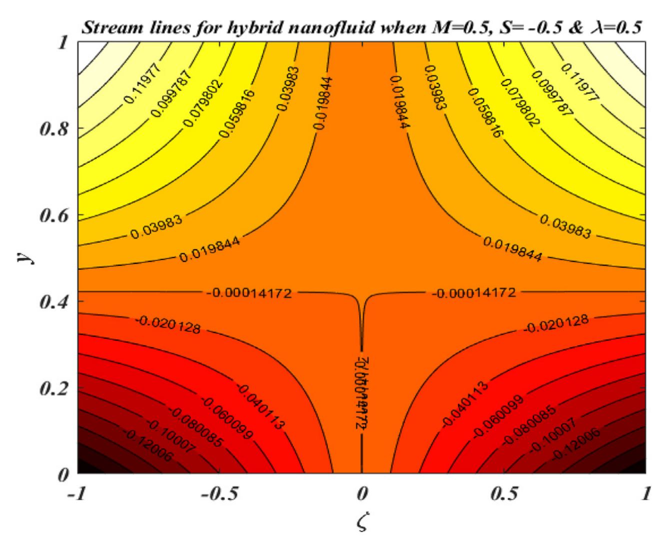

Fig. 17 Variation of streamlines when $M = 0.5$ for$S = -0.5\&\lambda = 0.5$.

nanoparticles with hybrid particles and base fluid ethylene glycol. The temperature distribution filed $\theta(\zeta)$ boosted by increment in the values of$(\phi_1 = \phi_2)$.The stimulus of (Ω) on $\theta(\zeta)$ is displayed in Fig. 10**.** It can be detected from the figure that the enhanced (Ω) refuses the temperature distribution filed $\theta(\zeta)$ for various shape factors of nanoparticles with the base fluid being ethylene glycol.Fig. 11 shows that the thermal profile is a higher magnitude for Lamina (16.1576) and a low magnitude for the sphere(3.000).The importance of (M) on (N_G) is seen in Fig. 12**.** As the entropy distribution filed (N_G) improves with mounting magnitudes of the magnetic parameter. This is owing to the Lorentz force, which is a resistance force that crosses the fluid motion, causing heat to be produced. As a result, as the magnetic field becomes larger, both the boundary layer thickness and the entropy distribution of filed (N_G) boundary layer increase. The outcomes of entropy distribution filed (N_G) for larger velocity slip (λ) are addressed in Fig. 13**.** It is perceived that the entropy distribution filed (N_G) dwindles for higher velocity slip parameter (λ) for various shape factors of nanoparticles with hybrid nanofluid and base fluid is ethylene glycol. Inspiration of the volumetric fraction of nanoparticles $(\phi_1 = \phi_2)$ on the entropy distribution filed (N_G) is disclosed in Fig. 14**.** It is predicted that the entropy distribution filed (N_G) can be lowered by increasing the flow behavior of the volumetric fraction of nanoparticles $(\phi_1 = \phi_2)$ for various shape factors of nanoparticles with hybrid particles and base fluid is ethylene glycol. Fig. 15 is prepared to interpret

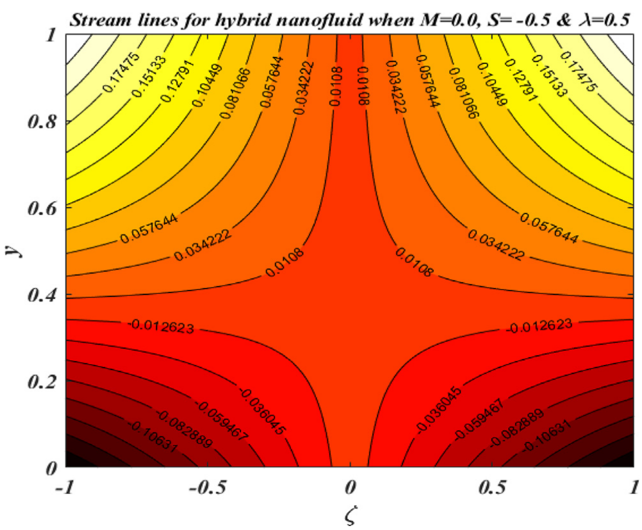

Fig. 18 Variation of streamlines when $M = 0.0$ for$S = -0.5\&\lambda = 0.5$.

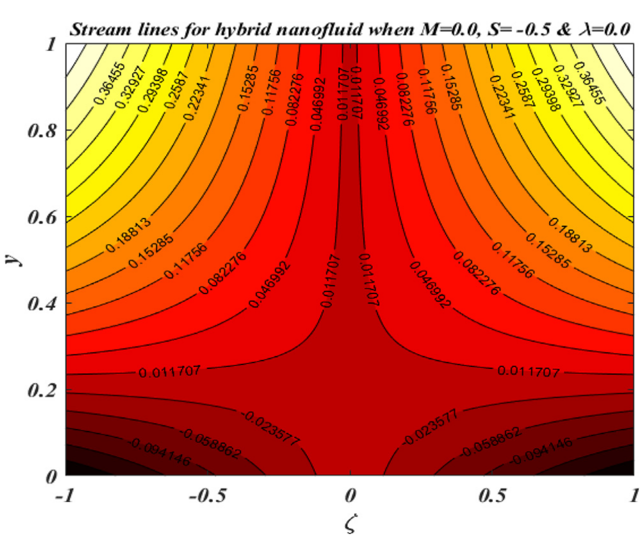

Fig. 19 Variation of streamlines when $M = 0.0$ for$S = -0.5\&\lambda = 0.0$.

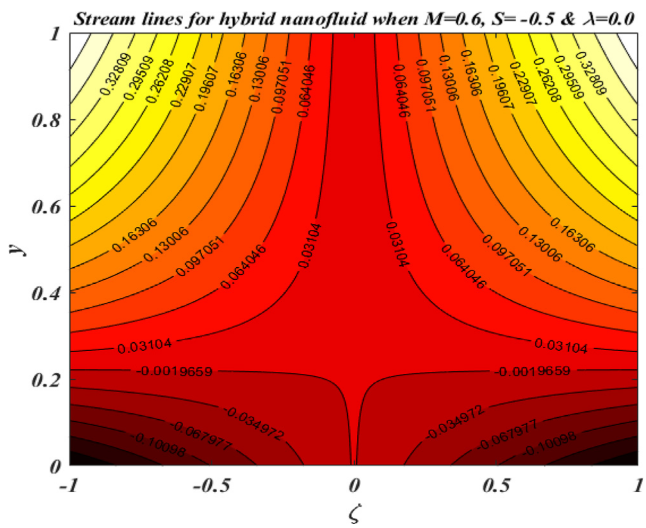

Fig. 20 Variation of streamlines when $M = 0.6$ for$S = -0.5\&\lambda = 0.0$.

Table 2 Experimental values of nanoparticles.

Properties	Density	Heat Capacity	Thermal Conductivity	Electrical Conductivity
(Fe_3O_4) 	5180	670	9.7	0.74×10^6
$(SWCNT)$ 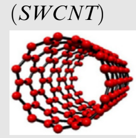	2600	425	6600	–
$(MWCNT)$ 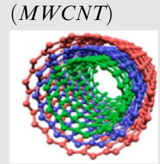	1600	796	3000	–
(EG) 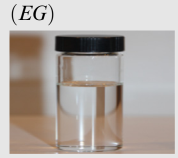	1114	2415	0.2525	5.5×10^{-6}

Table 3 Shape factor of nanoparticles (Raza Shah Naqvi et al., 2022).

Geometrical appearance	Shape Factor
 (Brick)	3.7
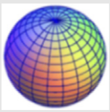 (Sphere)	3.0
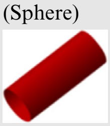 (Cylinder)	4.9
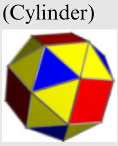 (Hexahedron)	3.7221
 (Tetrahedron)	4.0613
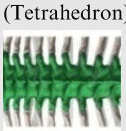 (Column)	6.3598
 (Platelet)	5.7
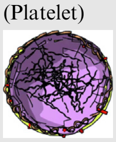 (Lamina)	16.1576

the deviation in entropy distribution filed (N_G) for Reynolds number (Re) for various shape factors of nanoparticles with hybrid nanoparticles and base fluid is ethylene glycol. From the curves of entropy, it is depicted that the entropy distribution filed (N_G) boosted up with a larger Reynolds number(Re). The variation of entropy distribution filed (N_G) with Brinkman number (Br) is reported in Fig. 16. It is interpreted that the entropy distribution filed (N_G) increased for larger Brinkman numbers (Br) for various shape factors of nanoparticles with $(SWCNT - Fe_3O_4, MWCNT - Fe_3O_4)$ and base fluid is ethylene glycol. Fig. 17 shows the variation of streamlines when the $(M = 0.5)$ for$(S = -0.5\&\lambda = 0.5)$. Fig. 18 analyzes the estimations of streamlines when $(M = 0.0)$ for$(S = -0.5\&\lambda = 0.5)$. Fig. 19 studied the impacts of streamlines when the magnetic parameter $(M = 0.0)$ for$(S = -0.5\&\lambda = 0.0)$. Fig. 20 investigates the aspects of streamlines when $(M = 0.6)$ for$(S = -0.5\&\lambda = 0.0)$. Table 1 shows the physical characteristics of nanofluid and hybrid nanofluid like as density, thermal conductivity, viscosity, and heat capacity. Table 2 displays the experimental magnitudes of nanoparticles like Carbon nanotube (SWCNT & MWCNT), Ferro (Fe_3O_4), and base fluid ethylene glycol. Table 3 analyzed the shape factor including such (brick sphere, cylinder, hexahedron, tetrahedron,column, platelet, and lamina). Table 4 shows the comparison of the Pr over the Nusselt number for the current fluid model. It shows good validations between the old and current frameworks.

6. Concluding remarks

In the current computational and numerical investigation we investigated the significance of thermal radiation on hybrid nanofluid having nanoparticles $(SWCNT, MWCNT\&Fe_3O_4)$ and base fluid (EG) ethylene glycol passing through a starching sheet. The outcomes of Cattaneo–Christov heat theory and entropy generation are also studied here. We use the Keller box numerical technique in the computational tool MATLAB to find the outcomes of prominent flow parameters via momentum profile, thermal field, and entropy profile. The main results of the current framework are listed here.

- The velocity field is declined when the velocity slip parameter is enhanced.
- For an enhanced magnitude of magnetic parameter and a volumetric proportion of nanoparticles, the velocity distribution field decreases.
- The temperature distribution field is improved for the advanced values of the thermal radiation parameter and(λ).
- The thermal field is increased for the growing estimations of thermal relaxation parameter.
- The entropy generation field is reduced for the raising magnitude of $(\phi_1 = \phi_2)$ and velocity slip parameter.
- The entropy generation field is boosted up for the growing magnitudes of both parameters Brinkman number and(Re).
- The main application of the currently analyzed hybrid nanofluid in neurological diseases is because carbon nanotubes are more useful for this.

Table 4 Comparison of Prandtl number over Nusselt number for the current fluid model.

Pr	Ishak et al. (Ishak et al., 2009)	Abolbashari et al. (Abolbashari et al., 2014)	Das et al. (Das et al., 2015)	Jamshed & Aziz (Jamshed and Aziz, 2018)	Current work
0.7	0.8086	0.80863135	0.80876122	0.80876181	0.80876182
1.0	1.0000	1.00000000	1.00000000	1.00000000	1.00000000
3.0	1.9236	1.92368259	1.92357431	1.92357420	1.92357421
7.0	3.0722	3.07225021	3.07314679	3.07314651	3.07314652
10.0	3.7006	3.72067390	3.72055436	3.72055429	3.72055430

- Because of the particle's use in engineering and manufacturing for expanding and contracting shells, such as packaging, sheet polymerization, glass fiber production, bundle wrapping, hot roll, metallic packages, and aluminum bottles industrial production, wire roll, parabolic difficult surface collectors, cooling of thermal reactors, and so on, the investigation oftwo-dimentional flowing over a sheet has been conducted. The proposed problem findings are used to increase heat transfer in a variety of liquids by utilizing nanoparticles and phenomena such as nonlinear thermal radiation and Cattaneo-Christov heat flux.

Declaration of Competing Interest

The authors declare that they have no known competing financial interests or personal relationships that could have appeared to influence the work reported in this paper.

References

Abolbashari, M.H., Freidoonimehr, N., Nazari, F., Rashidi, M.M., 2014. Entropy analysis for an unsteady MHD flow past a stretching permeable surface in nano-fluid. Powder Technol. 267, 256–267.

Ahmad, M., Imran, M.A., Nazar, M., 2020. Mathematical modeling of (Cu– Al2O3) water-based Maxwell hybrid nanofluids with Caputo-Fabrizio fractional derivative. Adv. Mech. Eng. 12 (9). 1687814020958841.

Aziz, A., Jamshed, W., Aziz, T., Bahaidarah, H., Ur Rehman, K., 2021. Entropy analysis of Powell-Eyring hybrid nanofluid including the effect of linear thermal radiation and viscous dissipation. J. Therm. Anal. Calorim. 143 (2), 1331–1343.

Biswas, N., Manna, N.K., Chamkha, A.J., 2021. Effects of half-sinusoidal nonuniform heating during MHD thermal convection in Cu–Al2O3/water hybrid nanofluid saturated with porous media. J. Therm. Anal. Calorim. 143 (2), 1665–1688.

Brewster, M.Q., 1992. Thermal radiative transfer and properties. John Wiley & Sons.

Cebeci, T., Bradshaw, P., 2012. Physical and computational aspects of convective heat transfer. Springer Science & Business Media.

Chamkha, A.J., Dogonchi, A.S., Ganji, D.D., 2019. Magneto-hydrodynamic flow and heat transfer of a hybrid nanofluid in a rotating system among two surfaces in the presence of thermal radiation and Joule heating. AIP Adv. 9, (2) 025103.

Choi, S.U., Eastman, J.A., 1995. Enhancing thermal conductivity of fluids with nanoparticles (No. ANL/MSD/CP-84938; CONF-951135-29). Argonne National Lab.(ANL), Argonne, IL (United States).

Daniel, Y.S., Aziz, Z.A., Ismail, Z., Salah, F., 2017. Numerical study of Entropy analysis for the electrical unsteady natural magnetohydrodynamic flow of nanofluid and heat transfer. Chin. J. Phys. 55 (5), 1821–1848.

Daniel, Y.S., Aziz, Z.A., Ismail, Z., Salah, F., 2017. Effects of thermal radiation, viscous and Joule heating on electrical MHD nanofluid with double stratification. Chin. J. Phys. 55 (3), 630–651.

Daniel, Y.S., Daniel, S.K., 2015. Effects of buoyancy and thermal radiation on MHD flow over a stretching porous sheet using homotopy analysis method. Alex. Eng. J. 54 (3), 705–712.

Daniel, Y.S., Aziz, Z.A., Ismail, Z., Salah, F., 2017. Entropy analysis in electrical magnetohydrodynamic (MHD) flow of nanofluid with effects of thermal radiation, viscous dissipation, and chemical reaction. Theor. Appl. Mech. Lett. 7 (4), 235–242.

Daniel, Y.S., Aziz, Z.A., Ismail, Z., Salah, F., 2018. Impact of thermal radiation on electrical MHD flow of nanofluid over a nonlinear stretching sheet with variable thickness. Alex. Eng. J. 57 (3), 2187–2197.

Daniel, Y.S., Aziz, Z.A., Ismail, Z., Bahar, A., Salah, F., 2019. Stratified electron magnetohydrodynamic flow of nanofluid supporting convective role. Korean J. Chem. Eng. 36 (7), 1021–1032.

Daniel, Y.S., Aziz, Z.A., Ismail, Z., Salah, F., 2019. Thermal radiation on unsteady electrical MHD flow of nanofluid over a stretching sheet with chemical reaction. Journal of King Saud University-Science 31 (4), 804–812.

Das, S., Chakraborty, S., Jana, R.N., Makinde, O.D., 2015. Entropy analysis of unsteady magneto-nanofluid flow past accelerating stretching sheet with convective boundary condition. Appl. Math. Mech. 36 (12), 1593–1610.

Farooq, U., Waqas, H., Khan, M.I., Khan, S.U., Chu, Y.M., Kadry, S., 2021. Thermally radioactive bioconvection flow of Carreau nanofluid with modified Cattaneo-Christov expressions and exponential space-based heat source. Alex. Eng. J. 60 (3), 3073–3086.

Ghadikolaei, S.S., Yassari, M., Sadeghi, H., Hosseinzadeh, K., Ganji, D.D., 2017. Investigation on thermophysical properties of Tio2–Cu/H2O hybrid nanofluid transport dependent on shape factor in MHD stagnation point flow. Powder Technol. 322, 428–438.

Ghalambaz, M., Sabour, M., Pop, I., Wen, D., 2019. Free convection heat transfer of MgO-MWCNTs/EG hybrid nanofluid in a porous complex-shaped cavity with MHD and thermal radiation effects. Int. J. Numer. Meth. Heat Fluid Flow.

Hayat, T., Momani, S., Muhammad, K., 2021. FDM analysis for nonlinear mixed convective nanofluid flow with entropy generation. Int. Commun. Heat Mass Transfer 126, 105389.

Hussanan, A., Qasim, M., Chen, Z.M., 2020. Heat transfer enhancement in sodium alginate-based magnetic and non-magnetic nanoparticles mixture hybrid nanofluid. Physica A 550, 123957.

Ishak, A., Nazar, R., Pop, I., 2009. Boundary layer flow and heat transfer over an unsteady stretching vertical surface. Meccanica 44 (4), 369–375.

Jamshed, W., Aziz, A., 2018. Cattaneo-Christov based study of $ ${\text {TiO}} _2 $$ TiO 2–CuO/EG Casson hybrid nanofluid flow over a stretching surface with entropy generation. Appl. Nanosci. 8 (4), 685–698.

Kang, H.U., Kim, S.H., Oh, J.M., 2006. Estimation of thermal conductivity of nanofluid using experimental effective particle volume. Exp. Heat Transfer 19 (3), 181–191.

Keller, H.B., 1971. A new difference scheme for parabolic problems. In: Numerical Solution of Partial Differential Equations–II. Academic Press, pp. 327–350.

Li, Y., Waqas, H., Imran, M., Farooq, U., Mallawi, F., Tlili, I., 2020. A numerical exploration of modified second-grade nanofluid with motile microorganisms, thermal radiation, and Wu's slip. Symmetry 12 (3), 393.

Maraj, E.N., Iqbal, Z., Shaiq, S., 2018. The extraordinary role of hydrogen possessions and viscosity variation in electrically conducting copper and silver nanoparticles inspired by mixed convection. Int. J. Hydrogen Energy 43 (24), 10915–10925.

Maraj, E.N., Bibi, A., Ijaz, S., Mehmood, R., 2022. MHD Carbon Nanotubes Gravity-Driven Flow Along a Thermal Sensitive Porous Surface. Arab. J. Sci. Eng., 1–11

Maraj, E.N., Nadeem, S., 2016. Theoretical analysis of entropy generation in peristaltic transport of nanofluid in an asymmetric channel. Int. J. Exergy 20 (3), 294–317.

Muhammad, K., Hayat, T., Alsaedi, A., 2021. Numerical study of Newtonian heating in the flow of hybrid nanofluid (SWCNTs + CuO + Ethylene glycol) past a curved surface with viscous dissipation. J. Therm. Anal. Calorim. 143 (2), 1291–1302.

Muhammad, K., Hayat, T., Alsaedi, A., Ahmed, B., 2021. A comparative study for the convective flow of base fluid (gasoline oil), nanomaterial (SWCNTs), and hybrid nanomaterial (SWCNTs + MWCNTs). Appl. Nanosci. 11 (1), 9–20.

Muhammad, K., Hayat, T., Alsaedi, A., Ahmad, B., Momani, S., 2021. Mixed convective slip flow of hybrid nanofluid (MWCNTs +

Cu+ Water), nanofluid (MWCNTs+ Water) and base fluid (Water): a comparative investigation. J. Therm. Anal. Calorim. 143 (2), 1523–1536.

Muhammad, K., Hayat, T., Alsaedi, A., Ahmad, B., 2021. Melting heat transfer in squeezing flow of base fluid (water), nanofluid (CNTs+ water), and hybrid nanofluid (CNTs+ CuO+ water). J. Therm. Anal. Calorim. 143 (2), 1157–1174.

Mukhopadhyay, S., Vajravelu, K., Van Gorder, R.A., 2013. Casson fluid flow and heat transfer at an exponentially stretching permeable surface. J. Appl. Mech. 80 (5).

Mustafa, M., Khan, J.A., 2015. Model for the flow of Casson nanofluid past a non-linearly stretching sheet considering magnetic field effects. AIP Adv. 5, (7) 077148.

Nadeem, S., Maraj, E.N., 2014. The mathematical analysis for peristaltic flow of a nanofluid in a curved channel with compliant walls. Appl. Nanosci. 4 (1), 85–92.

Nasir, S., Shah, Z., Alrabaiah, H., Islam, S., Khan, S.N., 2020. MHD stagnation point flow of hybrid nanofluid over a permeable cylinder with homogeneous and heterogeneous reaction. Phys. Scr. 96, (3) 035201.

Oyelakin, I.S., Mondal, S., Sibanda, P., 2016. Unsteady Casson nanofluid flow over a stretching sheet with thermal radiation, convective, and slip boundary conditions. Alex. Eng. J. 55 (2), 1025–1035.

Raza Shah Naqvi, S.M., Farooq, U., Waqas, H., Muhammad, T., Alshehri, A., 2022. Inspection of thermal jump conditions on nanofluids with nanoparticles and multiple slip effects. Sci. Rep. 12 (1), 1–14.

Roşca, N.C., Roşca, A.V., Pop, I., 2020. The axisymmetric flow of hybrid nanofluid due to a permeable non-linearly stretching/shrinking sheet with radiation effect. Int. J. Numer. Meth. Heat Fluid Flow.

Shahzad, F., Baleanu, D., Jamshed, W., Nisar, K.S., Eid, M.R., Safdar, R., Ismail, K.A., 2021. Flow and heat transport phenomenon for dynamics of Jeffrey nanofluid past stretchable sheet subject to Lorentz force and dissipation effects. Sci. Rep. 11 (1), 1–15.

Shaiq, S., Maraj, E.N., 2019. Role of the induced magnetic field on dispersed CNTs in propylene glycol transportation toward a curved surface. Arab. J. Sci. Eng. 44 (9), 7515–7528.

Tian, M.W., Rostami, S., Aghakhani, S., Goldanlou, A.S., Qi, C., 2021. A techno-economic investigation of 2D and 3D configurations of fins and their effects on heat sink efficiency of MHD hybrid nanofluid with slip and non-slip flow. Int. J. Mech. Sci. 189, 105975.

Waqas, H., Farooq, U., Hassan, A., Liu, D., Noreen, S., Makki, R., Ali, M.R., 2023. Numerical and Computational simulation of blood flow on hybrid nanofluid with heat transfer through a stenotic artery: Silver and gold nanoparticles. Results Phys. 44, 106152.

Zainal, N.A., Nazar, R., Naganthran, K., Pop, I., 2020. MHD flow and heat transfer of hybrid nanofluid over a permeable moving surface in the presence of thermal radiation. Int. J. Numer. Meth. Heat Fluid Flow.